JOURNAL OF SOLID STATE CHEMISTRY 91, 339–349 (1991)

Neutron and X-Ray Rietveld Analysis of the Three Phases of Lead Orthovanadate $Pb_3V_2O_8$: Importance of the Electronic Lone Pairs in the Martensitic Transitions

J. M. KIAT*,†,‡, P. GARNIER,* AND M. PINOT†

*Laboratoire de Chimie-Physique du Solide, URA 453 au C.N.R.S., Ecole Centrale de Paris 92295 Châtenay-Malabry Cedex, France; and †Laboratoire Léon Brillouin (C.E.A.-C.N.R.S.), CEN-Saclay, 91191 Gif-sur-Yvette Cedex, France

Received June 11, 1990; in revised form November 20, 1990

Neutron and X-ray powder diffraction investigations have been performed for the three phases of $Pb_3V_2O_8$. The structural results from the Rietveld refinements are analyzed and compared with the available data of both phases of $Pb_3P_2O_8$. The rhombohedral high temperature structures consist of layers of $[PO_4]$ or $[VO_4]$ tetrahedra. Inside this skeleton of tetrahedra the lead atoms have bonds of different lengths with the oxygen atoms in order to adapt themselves to the packings. The layers of the structures are connected by the electronic lone pairs of the lead ions inside the interlayers. The different phase transitions of both compounds mainly differ by the way the steric occupation of the electronic lone pairs is realized inside the interlayers. The microscopic interpretation of the large shears observed during the martensitic-like transitions is explained on the basis of the tilting of the lone pairs at the critical temperatures.

Introduction

Lead orthovanadate $Pb_3(VO_4)_2$ (or $Pb_3V_2O_8$) displays two structural phase transitions at about 373 and 273 K (*1*) which have been the subject of many studies because of their highly first-order natures. Above 373 K it crystallizes in a rhombohedral γ phase with the space group $R\bar{3}m$ ($Z = 1$). Below this temperature the threefold symmetry is broken and the rhombohedral phase transforms into a monoclinic β phase with the space group $P2_1/c$ ($Z = 2$). Below 273 K the β phase transforms into another monoclinic α phase with the space group $A2$[1] ($Z = 2$) (*2*). These transitions have been characterized by means of electronic microscopy (*3*) and X-ray and neutron diffraction (*3–5*). However, the different structures are not exactly known: the low temperature α phase and the intermediate β phase have been the subject of an X-ray powder diffraction study, but the oxygen atoms could not be accurately located and therefore no interatomic distances can be calculated (*2*). Moreover, the high temperature γ phase is

‡ To whom correspondence should be addressed.

[1] The $A2$ space group has been chosen instead of the equivalent $C2$ space group to conserve the same orientation for the cell axis for the β and the α phases. The comparison of the two phases is easier.

0022-4596/91 $3.00

supposed to be isotypic to the rhombohedral γ phase of the lead orthophosphate $Pb_3(PO_4)_2$ (or $Pb_3P_2O_8$). However, this isotypism has not been proven up to now. Despite this supposed isotypism, $Pb_3V_2O_8$ and $Pb_3P_2O_8$ present different phase transitions: below 453 K $Pb_3P_2O_8$ transforms into a monoclinic β' phase which remains stable down to 5 K with the $C2/c$ space group ($Z = 4$). This compound, for which structural data are available (*4, 6*), has been intensively studied because it is the first reported pure ferroelastic material and possesses a strong unusual pretransitional regime (*7–9*).

The γ, β, and α phases of $Pb_3V_2O_8$ are respectively paraelastic–paraelectric, ferroelastic–antiferroelectric, and ferroelastic–ferroelectric. The β' phase of $Pb_3P_2O_8$ is ferroelastic. All these transitions are high first order with strong volumetric discontinuities, especially $Pb_3V_2O_8$, and are characterized by important shears (Fig. 1).

It seems to us of interest to perform a structural determination of the different phases of the lead orthovanadate and to compare them with the phases of the lead orthophosphate. The aim of this study is to understand the structural evolutions and to try to draw a common mechanism for the different transitions.

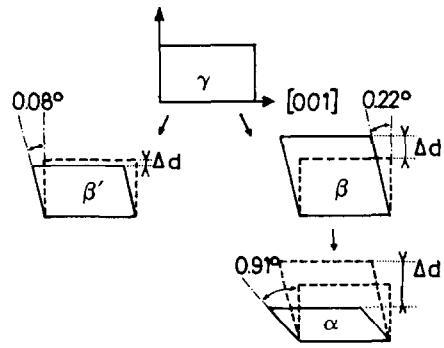

FIG. 1. Comparison of the shears at the critical temperatures for the different phase transitions of $Pb_3P_2O_8$ and $Pb_3V_2O_8$ in the **a, c** monoclinic plane of the common cell. The Δd jumps are 8×10^{-3}, 21×10^{-3}, and 45×10^{-3} Å, respectively, for the $\gamma \rightarrow \beta'$, $\gamma \rightarrow \beta$, and $\beta \rightarrow \alpha$ transitions.

Structural investigations were performed using both neutron and X-ray diffraction as it is the only way to get valuable information for vanadium and oxygen atoms beside lead atoms. The experiments were performed at 85, 300, and 585 K on powdered samples. Indeed a structural determination on a single crystal is not possible for $Pb_3V_2O_8$ for the following reasons: first, in contrast to $Pb_3P_2O_8$, synthesis of single crystals with sufficient size for neutron experiments has been unsuccessful up to now; second, as the transitions are strongly first order, even small single crystals are damaged when passing the critical temperatures; third, except in the rhombohedral phase, the crystals are always twinned because of the breaking of the threefold symmetry.

Experimental

Well-crystallized powder samples were synthesized by mixing PbO and V_2O_5 in the appropriate proportions and melting them in a platinum crucible at 1000°C in air for 1 hr. The melt was cooled (100 K · hr^{-1}) down to room temperature. After being ground, the samples were annealed at 700°C for 12 hr.

X-ray experiments were performed using a two-axis diffractometer (Bragg–Brentano geometry) whose angular accuracy is 10^{-3}°Θ (*10*). The Cu$K\alpha$ monochromatic radiation (graphite-bent monochromator) of a Rigaku anode (18 kW) was used. In order to avoid a very strong orientation effect the samples were sprinkled on an aluminum plaque covered by a grease film, for the room and low temperature experiments, and covered by a film of silver lacquer for the high temperature ones. The patterns were scanned through steps of 0.01° (2Θ), between 12° and 100° (2Θ) with a fixed-time counting of 15 sec. For the low temperature

experiments a He-cryostat with thermal stability of 0.1 K and precision within 1 K was used. For the high temperature experiments a Rigaku furnace with stability of 1 K and precision of 2 K was used.

Neutron experiments were performed at Léon Brillouin Laboratory using the Orphée reactor facilities on the two-axis diffractometer 3T2 with a wavelength of 1.226 Å. The patterns were scanned through steps of 0.05° (2Θ), between 6° and 110° (2Θ) with a counting rate of 60 sec. The thermal stability and precision of the low and high temperature apparatus were the same as in the X-ray experiments.

Refinements

Least-squares structure refinements were performed with the Rietveld analysis program DBW3.2 (*11*). In the γ $R\bar{3}m$ cell there are one lead atom Pb(1) in the "a" special Wyckoff position, one lead atom Pb(2), one vanadium atom, and one oxygen atom O(1) in the "c" special position, and one oxygen atom O(4) in general position. The starting values were the atomic coordinates of γ-$Pb_3P_2O_8$ obtained from Ref. (*4*). In the β ($P2_1/c$) and α($A2$) cells there is one lead atom Pb(1) in the "a" special Wyckoff position; all the other atoms (one lead Pb(2), one vanadium, and four oxygen atoms) are in general positions. For the β and α phases the starting coordinates were the refined values obtained from Ref. (*2*).

The neutron data, for which Gaussian lineshapes were satisfactorily used, allowed the determination of the positions of lead and oxygen atoms (no refinement of the positions of the vanadium atoms has been realized, at this step, because of the weakness of their diffusion length). The positions of the vanadium were then refined from the X-ray patterns for which pseudo-Voigt lineshapes were used. At the end of this second stage the lead positions were released and refined from the X-ray data: they show no significant deviations ($<2\sigma$) from those obtained with the neutron patterns.

The background was measured on each pattern outside of Bragg peaks and interpolated between these values. The number of refined structural parameters, the values of the different R agreement factors, and the refined cell parameters are listed in Table I.

TABLE I

AGREEMENT FACTORS AND REFINED CELL PARAMETERS FOR THE THREE PHASES OF $Pb_3V_2O_8$

	Neutron			X-Rays		
Temperature (K)	85	300	585	85	300	585
Space group	A2	$P2_1/c$	$R\bar{3}m$	$A2$	$P2_1/c$	$R\bar{3}m$
R_p (%)	4.32	3.64	4.51	10.02	9.44	7.80
R_{wp} (%)	5.68	4.60	5.80	12.99	12.95	10.67
R_{exp} (%)	3.06	1.82	2.20	3.41	3.40	5.13
R_B (%)	2.26	1.92	3.55	7.71	5.71	4.80
N	21	21	10	9	9	5
a(Å)	7.4637(3)	7.5172(2)	5.7695(6)	7.4622(3)	7.5171(3)	5.7766(3)
b(Å)	6.1951(3)	6.1084(2)		6.1928(2)	6.1074(2)	
c(Å)	9.3526(4)	9.5284(3)	20.4424(5)	9.3512(4)	9.5314(5)	20.4666(5)
β(°)	116.600(2)	115.190(3)		116.562(3)	115.200(3)	

Note. ESDs are given in parentheses and N is the number of structural refined parameters.

The R values (R_B, Bragg and R_{wp}, weighted profile) of the neutron refinements are quite satisfactory. The X-ray R_B factors are fair, whereas the profiles of the lineshapes in the X-ray refinements are more difficult to correctly define, as it is classically observed, because they are much sharper than those of the neutrons (typically $10 \times 10^{-2}°(2\Theta)$ instead of $25 \times 10^{-2}°(2\Theta)$) and so more sensitive to anisotropic widening.

Figure 2 illustrates the neutron profile of the α phase (the most debated one). We have represented the experimental profile $I(2\Theta)$ and the difference between the observed and the calculated profiles: the agreement is quite good. The refined atomic positions and the isotropic temperature factors (B) are reported in Table II. The B factors are those obtained from the neutron refinements; they are more reliable because the corresponding patterns are the largest of the sin Θ/λ values.

Results: Description of the Different Phases

In order to compare the phases of the two compounds, the cell parameters are also given in a common monoclinic cell which is that of the β' phase of $Pb_3P_2O_8$ (Table III). In the rhombohedral γ phase this common cell is all centered faces (F) in addition to algebraic relationships between the monoclinic parameters due to the threefold symmetry ($c = b\sqrt{3} = 3a \cos \beta$); in the β phase of $Pb_3V_2O_8$, only the B faces of this common cell remain centered, whereas in the α phase the common cell is again all centered faces (F) but without the relationships between the cell parameters. Data for $Pb_3P_2O_8$ are those obtained by a neutron diffraction study on powder (*4*). To give evidence of the different atomic shifts and for comparison of the structures the atomic positions calculated in the common cell are given in

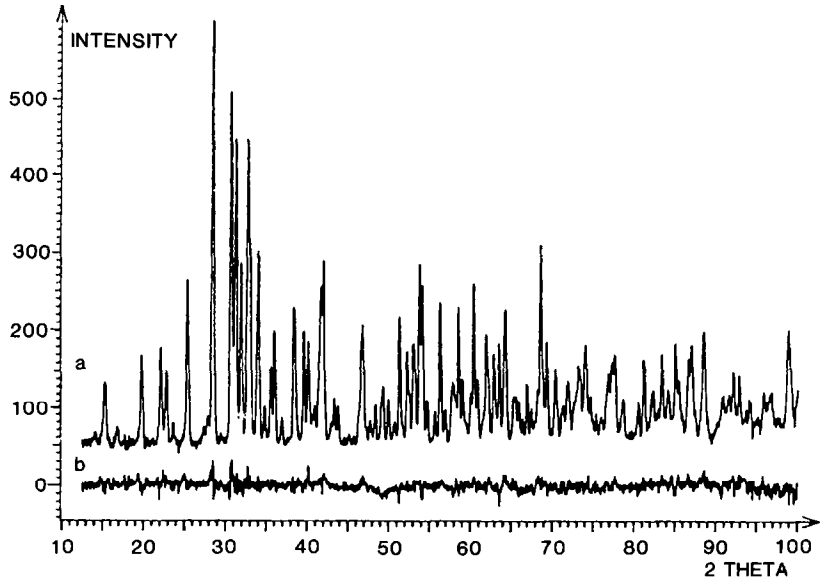

FIG. 2. Neutron diffraction profile for the α phase: (a) experimental profile, (b) difference between the observed and the calculated profiles.

TABLE II

$Pb_3V_3O_8$: LEAST-SQUARES REFINED ATOMIC COORDINATES IN THE USUAL CELLS AND ISOTROPIC THERMAL FACTORS (B *in* Å^2)

	γ-$Pb_3V_2O_8$ (585 K)	β-$Pb_3V_2O_8$ (300 K)	α-$Pb_3V_2O_8$ (85 K)
Pb(1)			
x	0	0	0
y	0	0	0
z	0	0	0
B	4.24(3)	2.46(8)	0.46(7)
Pb(2)			
x	0	0.3854(4)	0.3843(3)
y	0	0.5815(4)	0.5467(6)
z	0.2045(1)	0.2882(3)	0.2811(3)
B	5.51(2)	1.55(4)	0.70(5)
V			
x	0	0.2084(14)	0.2097(25)
y	0	0.0196(10)	0.0394(47)
z	0.4021(7)	0.4024(11)	0.4068(24)
B^a	0.70	0.70	0.70
O(1)			
x	−0.1606(4)	0.2880(7)	0.2368(6)
y	0.1606(4)	0.2568(8)	0.2960(8)
z	0.4314(2)	0.0206(6)	0.0447(5)
B	5.84(1)	1.85(9)	0.52(7)
O(2)			
x		0.2622(6)	0.3008(7)
y		0.7076(7)	0.7254(9)
z		0.0232(6)	0.0292(5)
B		1.16(10)	0.60(7)
O(3)			
x		0.3232(5)	0.3271(7)
y		0.9793(6)	0.9493(9)
z		0.2827(4)	0.2955(5)
B		1.20(7)	0.73(8)
O(4)			
x	0	0.0346(6)	0.0379(5)
y	0	0.5434(8)	0.5507(11)
z	0.3227(1)	0.2097(5)	0.2227(5)
B	3.66(1)	2.96(1)	1.00(7)

Note. ESDs are given in parentheses.
[a] Not refined.

Table III. The structure (Fig. 3) is also represented in this common cell.

γ *Phase*

The results obtained for the rhombohedral phase of $Pb_3V_2O_8$ confirm its isotypism with the orthophosphate phase. The structure can be described as a stacking of atomic layers orthogonal to the threefold axis (Fig. 3). These layers consist of two planes of $[VO_4]$ or $[PO_4]$ tetrahedra centered on $3m$ sites. In these tetrahedra three oxygen atoms (O_1, O_2, O_3) are connected by the threefold axis; the fourth oxygen atom (O_4) and the V (or P) atom are located on this axis. Two adjacent tetrahedra have their vertices in opposite positions; the stacking of these two types of tetrahedra defines the layer. Inside this skeleton of tetrahedra stand the lead atoms which are all located on the threefold axes. The Pb_1 atoms are in the median plane of the layers, on $\bar{3}m$ sites: they stand at the vertices of two tetrahedra with basal oxygen atoms (Fig. 4). The Pb_2 atoms are on $3m$ sites on the surfaces of the layers: they are connected inside the layer to an oxygen atom (O_4) of a $[VO_4]$ or $[PO_4]$ tetrahedron along a threefold axis and to an hexagon built up by oxygen atoms of the O_1, O_2, O_3 types. They are also connected to O_1, O_2, O_3 atoms of the opposite layer. Two opposite planes of Pb_2 atoms define the interlayer distance d_i (Fig. 3).

Our results show that there are important differences between the γ-$Pb_3V_2O_8$ and the γ-$Pb_3P_2O_8$ phases (Table IV). In the $[PO_4]$ or $[VO_4]$ tetrahedra the P–O distances (1.54 and 1.51 Å) are shorter than the V–O distances (1.70 and 1.66 Å) because of the different ionic radii (P^{5+}, 0.34 Å; V^{5+}, 0.59 Å). Moreover, whereas the nearest vicinity of the Pb_1 atoms is similar for the two compounds, this is not the case for the Pb_2 atoms: the shorter distance, i.e., Pb_2–O''_4, is smaller for $Pb_3P_2O_8$ (2.30 Å) than for $Pb_3V_2O_8$ (2.42 Å). Moreover the second shortest bonds are intralayer bonds for $Pb_3P_2O_8$ (with the oxygen atoms of the hexagon: 2.82 Å), whereas for $Pb_3V_2O_8$ they are with the three oxygen atoms of the opposite layers (2.78 Å).

TABLE III

ATOMIC COORDINATES GIVEN IN THE COMMON CELL (SEE TEXT)

	$Pb_3V_2O_8$			$Pb_3P_2O_8$[a]	
	γ (585 K)	β (300 K)	α (85 K)	γ (473 K)	β' (300 K)
a(Å)	14.0290(4)	13.9577(4)	13.6116(4)	13.89(1)	13.80(1)
b(Å)	5.7695(6)	6.1084(2)	6.1951(3)	5.530(2)	5.691(1)
c(Å)	9.9931(9)	9.5284(3)	9.3526(4)	9.58(1)	9.42(1)
β(°)	103.740(3)	102.914(3)	101.307(3)	103.3(1)	102.3(1)
Pb(1)					
x	0.5	0.5	0.5	0.5	0.5
y	0.75	0.75	0.75	0.75	0.791(2)
z	0.25	0.25	0.25	0.25	0.25
Pb(2)					
x	0.3067(2)	0.3073(2)	0.3078(2)	0.321(1)	0.317(1)
y	0.25	0.3315(2)	0.2967(6)	0.25	0.309(1)
z	0.3522(1)	0.3455(5)	0.3389(5)	0.357(1)	0.352(1)
V/P					
x	0.3941(11)	0.3958(7)	0.3951(12)	0.397(1)	0.401(1)
y	0.75	0.7696(10)	0.7894(5)	0.75	0.759(2)
z	0.5480(4)	0.5482(8)	0.5520(12)	0.549(1)	0.553(1)
O(1)					
x	0.1471(3)	0.1440(4)	0.1184(3)	0.141(1)	0.143(1)
y	0.5091(6)	0.5068(8)	0.5460(8)	0.523(1)	0.530(1)
z	0.3854(7)	0.3734(10)	0.3237(8)	0.388(1)	0.392(1)
O(2)					
x	0.1471(3)	0.1311(3)	0.1504(4)	0.141(1)	0.134(1)
y	0.9909(6)	0.9576(7)	0.9754(9)	0.977(1)	0.964(1)
z	0.3854(7)	0.3579(9)	0.3712(8)	0.388(1)	0.374(1)
O(3)					
x	0.1471(3)	0.1616(3)	0.1636(4)	0.141(1)	0.142(1)
y	0.25	0.2293(6)	0.1993(9)	0.25	0.220(2)
z	0.1263(5)	0.1289(7)	0.1181(8)	0.115(1)	0.112(1)
O(4)					
x	0.0160(2)	0.0173(3)	0.0190(3)	0.009(1)	0.009(1)
y	0.75	0.7934(8)	0.8007(11)	0.75	0.722(2)
z	0.0887(1)	0.0576(8)	0.0463(9)	0.086(1)	0.080(1)

[a] Data for $Pb_3P_2O_8$ are those of Ref. (*4*).

β Phase

During the $\gamma \rightarrow \beta$ phase transition the only important atomic shifts are those of the Pb_2 atoms (Table III) which essentially move along the twofold axis (*b*) in antiparallel directions (Fig. 5). All the Pb_1 atoms remain on a direction, orthogonal to the layers, which is a pseudo-threefold axis. The displacement of the Pb_2 atoms apart from this direction is important (0.50 Å). During the transition all the coordinance polyhedra of the V, Pb_1, and Pb_2 atoms lose their threefold symmetry.

The Pb_2 polyhedron gets a huge distortion (see Table IV). Inside the layers the bond lengths between the Pb_2 atoms and the oxygen atoms of the hexagon split into three groups of distances. The first one consists of two bonds (Pb_2–O_1'' and Pb_2–O_3'') which strongly diminish from 2.95 to 2.42 and 2.47 Å, respectively, and the second

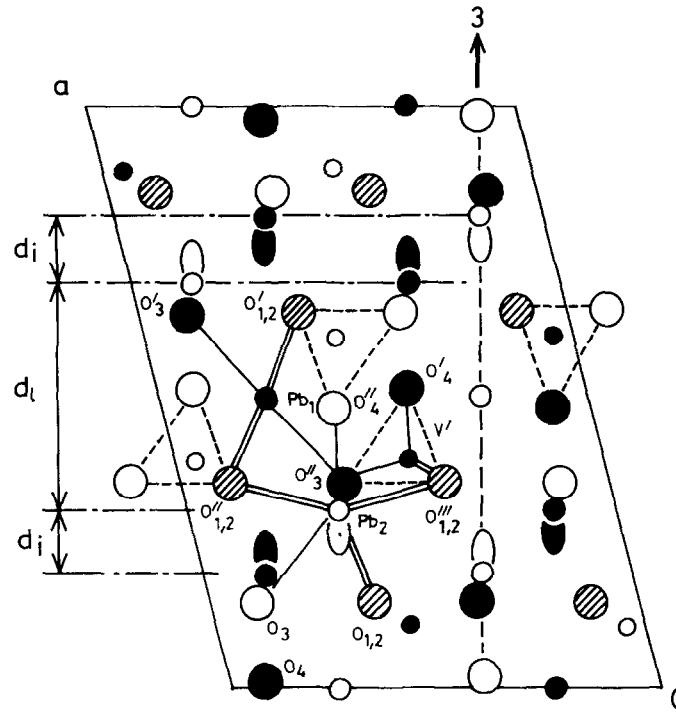

FIG. 3. Projection of the structure of the γ phase of $Pb_3V_2O_8$ in the monoclinic **a**,**c** plane of the common cell. The small, medium, and large circles represent respectively the vanadium, lead, and oxygen atoms, and the lobes represent the electron lone pairs. Open circles are located at $y = 1/4$, closed circles at $y = 3/4$, and hachured circles at $y \simeq 0$ and $\simeq 1/2$. The $[VO_4]$ tetrahedra are represented by dashed lines; d_l and d_i are the layer thickness and interlayer distances, respectively.

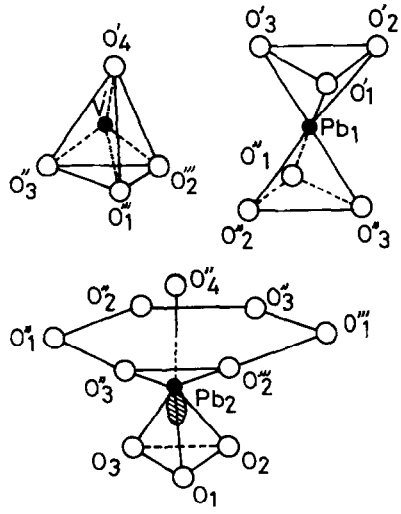

FIG. 4. Polyhedra of Pb_1, Pb_2, and V or P atoms in the γ phase.

one consists of two intermediate bonds (Pb_2–O''_2 and Pb_2–O'''_2) which slightly increase from 2.95 to 3.06 and 3.05 Å. The third one consists of two distances (Pb_2–O'''_1 and Pb_2–O''_3) which strongly increase up to 3.33 and 3.71 Å and so correspond to very weak bonds in this phase. Moreover, two interlayer distances (Pb_2–O_1 and Pb_2–O_3) shorten whereas the third (Pb_2–O_2) strongly increases (from 2.78 to 3.38 Å). During the transition the Pb_2–O''_4 distance remains constant (2.42 Å). Polyhedra of both vanadium and Pb_1 atoms display only a weak distortion: the main variation is for the Pb_1–O'_3 bond which increases from 2.65 to 2.76 Å.

α Phase

As for the $\gamma \rightarrow \beta$ transition the main atomic movements are again those of Pb_2

TABLE IV

BOND DISTANCES[a] IN Å AND ESDs (IN PARENTHESES)

	$Pb_3V_2O_8$			$Pb_3P_2O_8$[b]	
	γ (585 K)	β (300 K)	α (85 K)	γ (473 K)	β' (300 K)
V′/P′					
O_1'''	1.700(17)	1.708(24)	1.584(25)	1.54(3)	1.49(4)
O_2'''	1.700(17)	1.737(22)	1.940(24)	1.54(2)	1.57(3)
O_3''	1.700(17)	1.716(19)	1.726(26)	1.54(3)	1.56(3)
O_4'	1.660(20)	1.685(20)	1.699(25)	1.51(4)	1.47(4)
Pb_1					
O_1'(×2)	2.645(9)	2.599(10)	2.731(11)	2.58(2)	2.71(2)
O_2'(×2)	2.645(9)	2.612(12)	2.449(9)	2.58(2)	2.53(2)
O_3'(×2)	2.645(9)	2.757(18)	2.767(10)	2.58(2)	2.60(2)
Pb_2					
O_1	2.777(7)	2.586(13)	2.986(13)	2.99(3)	2.81(4)
O_2	2.777(7)	3.378(12)	2.984(15)	2.99(3)	3.24(3)
O_3	2.777(7)	2.628(15)	2.627(18)	2.99(3)	2.98(4)
O_1'''	2.953(9)	3.330(14)	3.321(15)	2.82(2)	3.05(2)
O_2'''	2.953(9)	3.049(15)	3.479(16)	2.82(2)	2.84(2)
O_3''	2.953(9)	2.471(7)	2.544(12)	2.82(2)	2.41(3)
O_1''	2.953(9)	2.416(17)	2.419(18)	2.82(2)	2.53(3)
O_2''	2.953(9)	3.063(18)	2.516(17)	2.82(2)	2.94(3)
O_3''	2.953(9)	3.706(7)	3.735(13)	2.82(2)	3.40(2)
O_4''	2.416(6)	2.427(14)	2.391(14)	2.30(4)	2.40(4)

[a] Superscripts and exponents refer to Figs. 3, 4, and 6.

[b] Distances for $Pb_3P_2O_8$ have been calculated from Ref. (*4*).

atoms along the twofold axis; however, they are now all in the same direction (0.30 Å, see Fig. (5)). As in the β phase the Pb_2 tetrahedron gets a large distortion. Inside the layers, the bonds of the Pb_2 atoms with the oxygen atoms of the hexagon are now split into two groups of short and long distances. The first group consists of the two short distances of the β phase (Pb_2–O_1'' and Pb_2–O_3'') which are almost not affected by the transition (2.42 and 2.54 Å instead of 2.42 and 2.47 Å), plus the Pb_2–O_2'' distance which strongly shortens (2.52 instead of 3.06 Å). The second group consists of the previous long distances of the β phase (Pb_2–O_1''' and Pb_2–O_3''), almost not affected (3.32 and 3.74 Å instead of 3.33 and 3.71 Å), plus the Pb_2–O_2''' distance which strongly increases (3.48 instead of 3.05 Å). As for the β phase the Pb_2–O_4'' bond gets only weak variation (2.42 to 2.39 Å). With the opposite layer one bond (Pb_2–O_3) remains unaffected (2.63 Å) and the two others (Pb_2–O_1 and Pb_2–O_2) become almost equal (2.98 Å). The distortions, in the Pb_1 polyhedron, remain weak: the main variations are the increase of the Pb_1–O_1' bond (2.60 to 2.73 Å) and the decreasing of the Pb_1–O_2' bond (2.61 to 2.45 Å). The vanadium polyhedron gets a larger distortion than in the β phase: one (V′–O_1''' bond diminishes from 1.71 to 1.58 Å, another one increases from 1.74 to 1.94 Å.

β′ Phase

Contrary to the $\gamma \rightarrow \beta \rightarrow \alpha$ phase transitions of $Pb_3V_2O_8$ the important shifts apart from the pseudo-threefold axis during the $\gamma \rightarrow \beta'$ transformation are those of both Pb_1

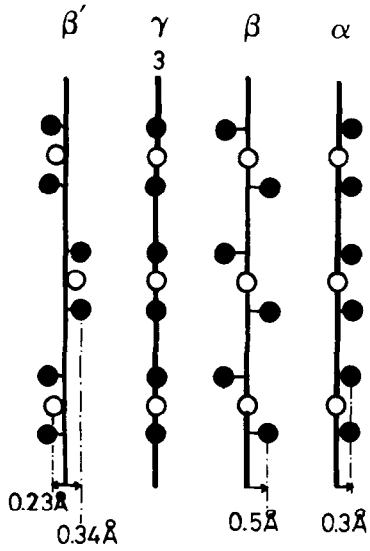

FIG. 5. Shifts at the transitions, along the **b** monoclinic axis apart from the threefold axis, of the Pb_1 (open circles) and Pb_2 (closed circles) atoms.

and Pb_2 (respectively 0.34 and 0.23 Å, see Fig. 5). As in the transitions of $Pb_3V_2O_8$ the main distortions are in the Pb_2 polyhedron. Inside the layer the Pb_2 bonds with the oxygen atoms of the hexagon split into three groups: the first group, corresponding to short distances, is the same as in the β phase (i.e., the Pb_2–O_1'' and Pb_2–O_3'' bonds which diminish from 2.82 to 2.53 and 2.41 Å). The second group consists of three intermediate distances: the Pb_2–O_2'' (2.94 Å) and the Pb_2–O_2''' (2.84 Å) as in the β phase, plus the Pb_2–O_1''' bond (3.05 Å). The third group consists of the long Pb_2–O_3'' distance (3.40 Å). In contrast to the β and α phases, the Pb_2–O_4'' bond shows a significant increase at the $\gamma \rightarrow \beta'$ transition (2.30 to 2.40 Å). Concerning the bonds with the oxygen atoms in the opposite layer, the Pb_2–O_3 length remains almost unaffected (2.98 Å instead of 2.99 Å), the Pb_2–O distance shortens (2.81 Å), and the Pb_2–O_2 distance increases (3.24 Å). The phosphorus and Pb_1 polyhedra are not affected very much by the transition: the most important variation is for the Pb_1–O_1' bond, which increases from 2.58 to 2.71 Å.

Discussion

It is well known that the divalent Pb^{II} atoms have an electronic lone pair whose barycenter is not obviously on the nucleus center, depending on the lead coordination polyhedron. This lone pair can occupy a very large steric volume: for instance, the polyhedron of lead oxide PbO is a square base pyramid of oxygen atoms with a Pb atom at the vertex, and the lone pair occupies a steric volume equivalent to that of an oxygen atom. A mechanism based on the existence of interactions between the lone pairs has been used to explain the phase transitions of some oxides like Pb_3O_4 (*12*) and PbO (*13*). In the case of α-PbO the incommensurate phase was shown to be characterized by an helicoidal modulation of the electronic lone pair shifts (*14*).

In the γ phase of $Pb_3V_2O_8$ and $Pb_3P_2O_8$ the Pb_1 atoms are on centrosymmetric $\bar{3}m$ sites: the lone pairs are centered on the nucleus. On the contrary the Pb_2 atoms are on the noncentrosymmetric site $3m$. The observation of the Pb_2 polyhedron shows that the lone pair is thrown off center, toward the interlayer space (Figs. 3 and 4), mainly because of the short Pb_2–O_4'' bond. The lone pair lies along the threefold axis, orthogonally to the layers, and occupies the room in the interlayer space (d_i). Two of them in adjacent layers are opposite and are responsible for a weak lead–lead interaction between these layers. In the case of γ-$Pb_3P_2O_8$ the Pb_2–O_4'' bond is shorter than that of γ-$Pb_3V_2O_8$; the hexagon of the oxygen atoms is closer whereas the three other oxygen atoms in the opposite layer are further. This involves for $Pb_3P_2O_8$ a stronger delocalization of the lone pair, and thus, a larger interlayer distance d_i (Table V). However, the structure of lead phosphate is globally more compact ($d_i + d_1$ is shorter)

TABLE V

LAYER THICKNESS AND INTERLAYER DISTANCES (Å)

	$Pb_3V_2O_8$			$Pb_3P_2O_8$[a]	
	γ (585 K)	β (300 K)	α (85 K)	γ (473 K)	β' (300 K)
Layer (d_l)	5.27	5.24	5.13	4.84	4.93
Interlayer (d_i)	1.55	1.56	1.54	1.92	1.81
Total distance ($d_l + d_i$)	6.82	6.80	6.67	6.76	6.74

[a] For $Pb_3P_2O_8$ the distances are calculated from Ref. (*4*).

than the lead vanadate structure, because its skeleton consists of the stacking of $[PO_4]$ tetrahedra smaller than $[VO_4]$ tetrahedra.

During all the phase transitions the vanadium (or the phosphorus) and the Pb_1 polyhedra are less distorted than the Pb_2 polyhedra. Moreover, in all the phases, the Pb_1 site remains centrosymmetric and those of Pb_2 noncentrosymmetric. As the Pb_2 polyhedra become highly distorted this causes a tilt of the lone pairs with respect to the direction perpendicular to the layers (i.e., the pseudo-threefold axis). This is evidenced when projecting the Pb_2 polyhedra on the **b, c** monoclinic plane of the common cell for the different monoclinic phases and comparing with the projection of the rhombohedral phases (Fig. 6). In the β phase the lead atom is shifted along a direction close in projection to $-\mathbf{b} + \mathbf{c}$, and therefore its bond lengths with the O_1'' and O_3'' atoms inside the layer diminish. Consequently the lone pair is thrown away and tilts in the opposite direction. In the α phase the projection of the lead atom displacement is almost along the **c** vector, the bond lengths with O_1'', O_2'', and O_3'' atoms inside the layer diminish; thus the lone pair tilts along the direction $-\mathbf{c}$. In the β' phase the direction of lead displacement in projection is very near the **b** direction, so the tilting of the lone pair is along the $-\mathbf{b}$ direction.

Our results show that the different transformations from the rhombohedral phase correspond to different possibilities of tilting for the lone pairs. In other words the monoclinic phases differ essentially by the way the steric occupation of the electronic lone pairs is realized inside the interlayers. In the case of γ-$Pb_3P_2O_8$ the interlayer distance d_i is large and is strongly reduced at the critical temperature: the β' phase corresponds to a weaker delocalization of the pairs obtained mainly by an increase of the Pb_2–O_4'' distance, and to a tilting along the b direction. In the case of γ-$Pb_3V_2O_8$ the interlayer distance d_i is lower and cannot be

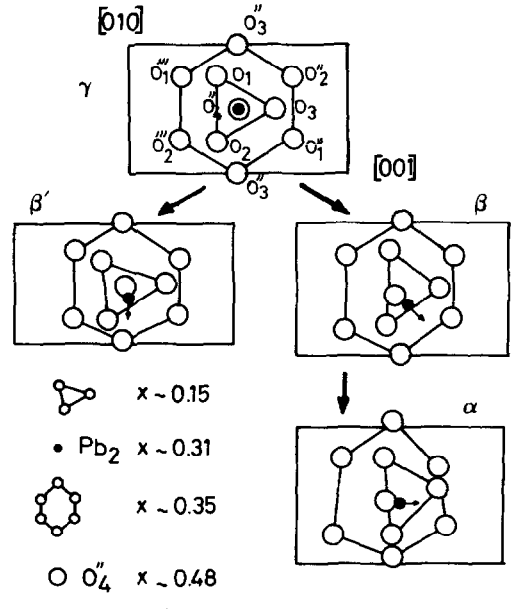

FIG. 6. Projection in the **b,c** monoclinic plane of the Pb_2 polyhedron in the different phases. The arrows represent the direction of the Pb_2 atom relative shifts.

significantly reduced: it remains almost constant during the $\gamma \rightarrow \beta \rightarrow \alpha$ transitions (and coherently also the Pb_2–O_4'' distance). Thus the β and α phases result from large tiltings of the pairs mainly along the **c** direction, which determine the huge shear of these two phases (Fig. 1), particularly for the α phase, the lone pair tilt being in the **a**, **c** plane.

To summarize both sequences, the $\gamma \rightarrow \beta'$ transition allows a large decrease of d_i and a small shear; the $\gamma \rightarrow \beta \rightarrow \alpha$ transitions allow very strong shears but no significant change for the interlayer distance d_i.

In conclusion the results of the refinements show that the different structures consist of a stacking of $[PO_4]$ or $[VO_4]$ tetrahedra. These tetrahedra remain relatively rigid during the different phase transitions. Inside this skeleton of tetrahedra the lead atoms have bonds of different lengths with the oxygen atoms in order to adapt themselves to the structures. During all the different phase transitions the only important movements are those of lead atoms. This analysis shows that a common mechanism for the phase transitions does exist; the existence of delocalized lone pairs for the lead atoms and the different ways they pack inside the structure is clearly correlated with the structural evolution of $Pb_3V_2O_8$ and $Pb_3P_2O_8$. The microscopic interpretation of the large shears at the critical temperatures comes from the existence of compact layers in the structure which are only connected by weak interactions between the pairs through the interlayers. This explains the similarities of the transitions of these insulating compounds with those of metals and alloys (martensitic transformations) where weak electronic interactions are involved. The presence of the electron lone pairs has to be correlated with the influence of pressure on lead orthovanadate phase transitions (*15*). In another paper we will report on the structural consequences of the substitution of phosphorus for vanadium.

Acknowledgment

The authors thank B. Rieu for his kind assistance during the neutron experiments.

References

1. V. A. Isupov, N. N. Krainik, I. D. Fridberg, and I. E. Zelenkova, *Sov. Phys. Solid State* **24**(5), 844 (1965).
2. P. Garnier, G. Calvarin, J. F. Berar, and D. Weigel, *Mater. Res. Bull.* **19,** 407 (1984).
3. C. Manolikas and S. Amelinckx, *Phys. Status Solidi A* **60,** 607 (1980).
4. D. M. C. Guimaraes, *Acta Crystallogr. Sect. A* **35,** 108 (1979).
5. J. M. Kiat, G. Calvarin, P. Garnier, and P. Gregoire, *J. Phys.* **48,** 253 (1987).
6. H. N. Ng and C. Calvo, *Can. J. Phys.* **53**(1), 42 (1975).
7. J. P. Benoit, B. Hennion, and M. Lambert, *Phase Trans.* **2,** 102 (1981).
8. I. G. Wood, V. K. Wadhawan, and A. M. Glazer, *J. Phys. C: Solid State Phys.* **13,** 5155 (1980).
9. E. Salje and V. Devarajan, *J. Phys. C: Solid State Phys.* **14,** L1029 (1981).
10. J. F. Berar, G. Calvarin, and D. Weigel, *J. Appl. Crystallogr.* **13,** 201 (1980).
11. D. B. Wiles and R. A. Young, *J. Appl. Crystallogr.* **14,** 149 (1981).
12. J. R. Gavarri, D. Weigel, and A. W. Hewat, *J. Solid State Chem.* **23,** 327 (1978).
13. J. P. Vigouroux, G. Calvarin, and E. Husson, *J. Solid State Chem.* **45,** 343 (1982).
14. A. Hedoux, D. Grebille, and P. Garnier, *Phys. Rev. B,* **40,** 15, 10633 (1989).
15. M. Midorikawa, H. Kashida, and Y. Ishabashi, *J. Phys. Soc. Jpn.* **50**(5), 1592 (1980).